2024 IEEE International Conference on Robotics and Automation (ICRA 2024)
May 13-17, 2024. Yokohama, Japan

Liquids Identification and Manipulation via Digitally Fabricated Impedance Sensors

Junyi Zhu*[1], Young Joong Lee*[1], Yiyue Luo*[1], Tianyu Xu[1,2], Chao Liu[1], Daniela Rus[1], Stefanie Mueller[1], and Wojciech Matusik[1]

***Abstract*— Despite recent exponential advancements in computer vision and reinforcement learning, it remains challenging for robots to interact with liquids. These challenges are particularly pronounced due to the limitations imposed by opaque containers, transparent liquids, fine-grained splashes, and visual obstructions arising from the robot's own manipulation activities. Yet, there exists a substantial opportunity for robotics to excel in liquid identification and manipulation, given its potential role in chemical handling in laboratories and various manufacturing sectors such as pharmaceuticals or beverages. In this work, we present a novel approach for liquid class identification and state estimation leveraging electrical impedance sensing. We design and mount a digitally embroidered electrode array to a commercial robot gripper. Coupled with a customized impedance sensing board, we collect data on liquid manipulation with a swept frequency sensing mode and a frequency-specific impedance measuring mode. Our developed learning-based model achieves an accuracy of 93.33% in classifying 9 different types of liquids (8 liquids + air), and 97.65% in estimating the liquid state. We investigate the effectiveness of our system with a series of ablation studies. These findings highlight our work as a promising solution for enhancing robotic manipulation in liquid-related tasks.**

I. INTRODUCTION

Robot manipulation has advanced dramatically thanks to the rapid development of computer vision and machine learning technologies. These breakthroughs empower robots to comprehend, anticipate, and engage with physical objects and their environments [1], [2], [3], [4]. Despite these strides, liquid manipulation continues to present challenges for conventional vision-based approaches. This is particularly evident when dealing with opaque containers, transparent liquids, splashes, and occlusions generated by the robot's own manipulative actions, where capturing visual information becomes inherently complex [5], [6].

To address these challenges, researchers have explored alternative sensing modalities, including vibration sensors [7], force sensors [8], infrared reflectance spectroscopy [9], and high-resolution tactile sensors [10], [11] for liquid manipulation. Despite the effectiveness of liquid identification and dynamics estimation, most of the introduced sensors require intricate and complex fabrication processes and are challenging to customize and scale up. In contrast, impedance-based sensing mechanisms, exemplified by electrical impedance tomography (EIT) and impedance spectroscopy, present a promising alternative. These methods leverage readily manufacturable electrodes, offer non-contact sensing capabilities, exhibit geometry-independent versatility, and can be scaled up through the addition of electrodes or sensor re-layout.

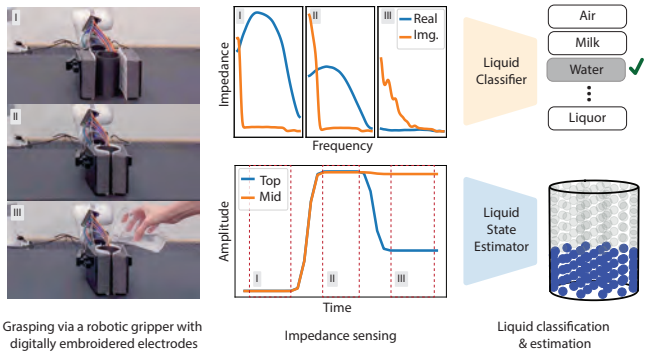

Fig. 1. **Pipeline overview.** We functionalize a parallel robotic gripper with a digitally embroidered impedance sensing array.

In this work, we present the leverage of impedance sensing via low-cost, scalable, customizable embroidered electrode arrays for liquid classification and state estimation. We digitally designed and automatically fabricated two distinct 4×4 electrode arrays using a digital embroidery machine. These electrode arrays are affixed to a parallel robotic gripper and serve as an impedance sensing matrix. We collected responses across swept frequencies and electrode pairs while manipulating and rotating containers filled with various liquids. We developed integrated models for liquid classification and liquid state estimation. We showcase the effectiveness of our framework with an accuracy of 93.33% in classifying 9 different types of liquids (8 liquids + air), and 97.65% in estimating the state of liquid. Our approach obtains potential for robotics manipulation of liquids, serving as a complementary sensing modality with well-established sensing systems, e.g., vision, for robots handling liquids with precision and efficiency.

II. RELATED WORK

A. Liquid Manipulation

Mimicking human-like proficiency in household tasks is a formidable challenge for robots, particularly when these tasks involve handling liquids. Extensive research has been dedicated to liquid manipulation, employing model-based control [12] or data-driven approaches [13], [14], where particular setup was built to avoid the complexities associated with fluid measurement during experiments. Accurate fluid measurement is critical for robots to autonomously execute

*Authors contributed equally to this work.

[1]Authors are with the Computer Science and Artificial Intelligence Laboratory (CSAIL), Massachusetts Institute of Technology, Cambridge, USA. [2]Authors are with Google, Mountain View, USA

pouring tasks with precision. Vision-based methods have been developed for flowing liquids detection, such as [15], [16], which provided useful information for robots to control liquid flow. To precisely control and transfer liquid between containers, the volume estimation could be helpful in building a feedback control loop. To this end, however, vision-based solutions (e.g., [17]) are limited due to the common occlusion in daily-life containers.

Taking inspiration from the way humans interact with their environment, the properties of liquid within a container can also be estimated using vision-based tactile sensors [10] and light-based spectroscopy [9]. These contact-based methods eliminate the challenges posed by visual occlusion, thus offering a significant advantage over vision-based feedback and ensuring more robust measurements. In addition, it has been shown that tactile sensors can be easily integrated into customized gripper designs [18]. This inspired our development of impedance-based sensing solutions for liquid measurement that can be directly mounted on a gripper.

B. Impedance Sensing for Robotics

Impedance sensing encompasses electrical impedance tomography (EIT) and electrical impedance spectroscopy (EIS). EIT noninvasively estimates the internal resistivity distribution based on the measured boundary voltage–current data [19]. It has been commonly used for medical applications such as lung function monitoring [20] and muscle engagement monitoring [21], [22], as well as industrial processing monitoring [23]. Recently, EIT has been extensively investigated as artificial skins for robotics due to its advantages of high versatility, low power consumption, and high sensitivity range [24]. Examples include single-layer rubber with conductive carbon particles as tactile sensing skins [25], [26], EIT-based flexible tactile sensing gloves for capturing human-object interactions [27], as well as using EIT as input for robotic prosthesis control [28]. On the other hand, EIS has been widely explored for material property detections [29] and battery characterization [30] in material science, and then the robotics community, such as via capacitive proximity sensor [31] and integrating with the robotic gripper for solid object material detection [32]. More recently, it has also been investigated for object and user behavior detections, which enables complex configurations of human hands and users' body recognization [33], [34].

In this work, we extend the benefits of low-cost and salable by digitally designing and integrating impedance sensing electrodes via digital machine embroidery. We leverage the inherent "see-through" capability of EIT and high versatility & wide frequency range impedance spectroscopy sensing for liquid type classification and state estimation.

III. METHOD

In this section, we present the details of our hardware and software development. We first discuss our sensor fabrication and coupled read-out circuit design. We then describe our data collection pipeline, ground truth generation, and model development for liquid classification and state estimation.

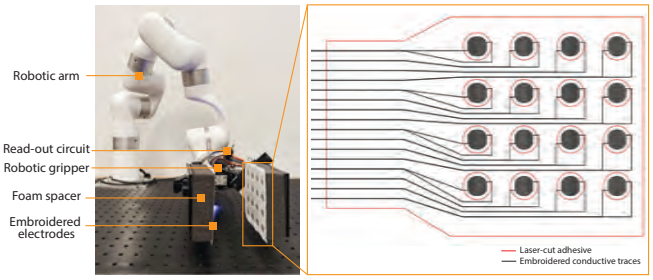

Fig. 2. **Embroidered impedance sensing matrix.** A 4×4 embroidered electrode array was affixed to each parallel gripper, with a foam spacer in between to enhance conformity during grasping. All electrode connections were routed to the edge for a convenient connection to the read-out circuit.

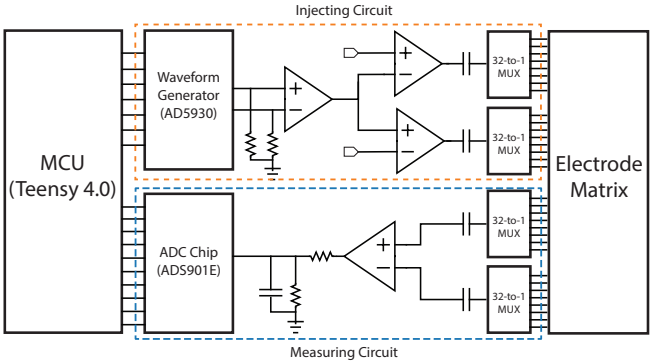

Fig. 3. **Read-out circuit diagram.**

A. Sensor Fabrication

Our impedance sensing matrix consists of two layers: a bottom layer with embroidered electrodes and connecting traces, and a top fabric layer with selective laser-cut spaces (Fig. 2). These spaces were designed to reveal the electrodes, allowing them to be in contact with the grasped objects, as well as to minimize cross-talk caused by the contact between the connecting traces and the objects. Our electrode matrices and the connecting traces were digitally designed and fabricated via digital embroidery (Taijima). To optimize impedance reading and minimize noise from the container, each electrode was embroidered with silver-plated polyamide thread (Madeira HC40) with a 10 mm diameter, 1 mm pitch, and 14 mm spacing from each other. The connection to each electrode was traced via conductive stitches to the side with a placement pitch of 2 mm. Such designs effortlessly interface with the read-out circuit via pre-fabricated connectors. Each of the electrode arrays obtained a 4×4 electrode matrix and was mounted to each side of the gripper with foam in between for conformal contact. With our fabrication pipeline, 4×4 electrode matrix takes less than 5 minutes to fabricate, which provides an opportunity for automated and scalable fabrication of such sensors. Our digital fabrication pipeline provides a remarkable advantage, allowing personalized adjustments in electrode sizes and placement to the unique geometries of robotic operators and meet the specific requirements of users.

B. Impedance Sensing Board

For better integration with the robotic grippers, we implemented a BLE-enabled customized impedance sensing

board (4cm×6cm), which is built around a Teensy 4.0 microcontroller, and responsible for injecting the AC signal and measuring the resulting voltage response via a 4×8 electrode matrix. The board has two modes: swept frequency sensing mode at pre-selected electrodes, and frequency-specific impedance measuring mode rotating through all connecting electrode pairs. As shown in Fig. 3, the impedance sensing board consists of two main parts: a current drive circuit for injecting the AC signal, and a voltage response measurement circuit for measuring the voltage output (i.e., signal amplitude and phase) from the current drive. On top of them, there is an additional control circuit built around the microcontroller that assigns the output of current injecting circuit & the input of voltage response measuring circuit to corresponding electrodes and processes the collected data.

Current Injecting Circuit: The current injecting circuit is composed of a signal generator, an adjustable instrumentation amplifier, and a voltage-controlled current source (VCCS). Specifically, the signal generator (AD5930) serves as a voltage source and generates a small, constant-amplitude, differential sine waveform at predefined frequencies based on frequency range and steps (frequency sweep mode), or at predetermined injection frequency (single frequency mode). The waveform is subsequently fed into the instrumentation amplifier (AD8220) and modulated by a digital rheostat (AD5270) to directly drive the VCCS. The resulting current output is differential and centered around 0, connected to a 4×8 electrode matrix via two separate 32-to-1 multiplexers (ADG731).

Voltage Response Measuring Circuit: The voltage response measuring circuit takes differential input from the 4×8 electrode matrix via two separate 32-to-1 multiplexers (ADG731). It is composed of two input buffers, an adjustable instrumentation amplifier, and a 10-bit analog-to-digital converter (ADC). Each of the two input buffers employs an op-amp (ADA4841) configured for unit-gain, followed by an RC high-pass filter with a 350Hz cutoff frequency. These buffers feed into the instrumentation amplifier (AD8220) followed by modulation from a digital rheostat (AD5270). The output voltage is scaled down from 5V to 3.3V and then passed through an RC band-pass filter with cutoff frequencies at 1kHz and 1MHz. Finally, the ADC chip (ADS901E) samples such filtered output at 20MHz and outputs voltage at 10 bits.

C. Data Collection

All data was collected by mounting our embroidered sensing matrix to a robotic gripper (Robotiq 2F-140), which was installed on a robotic arm (UFACTORY xArm). Data collection was conducted with two measurement setups: a swept frequency sensing mode with pre-selected electrodes, and a frequency-specific impedance measuring mode sampling across all connecting electrode pairs.

With a swept frequency sensing setup, we captured impedance signals with 4 electrodes (2 injecting electrodes and 2 measuring electrodes). The injecting electrode pair generated waveforms with a frequency sweeping from 5 kHz to 500 kHz (100 steps), and the measuring electrode

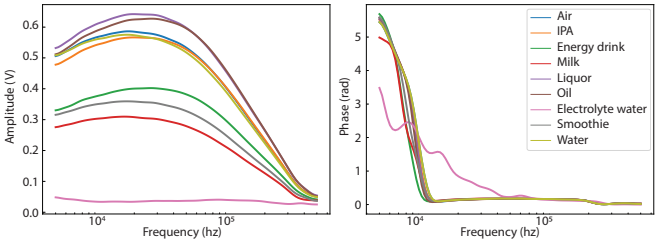

Fig. 4. **Sample impedance spectroscopy data for liquid classification.**

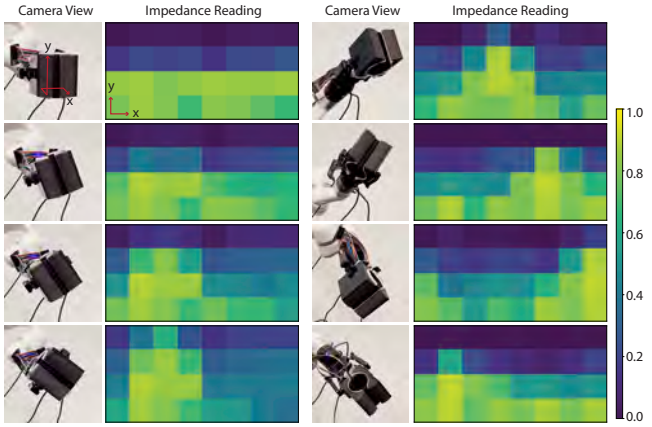

Fig. 5. **Representative impedance responses for liquid state estimation.** Impedance responses were captured by the embroidered electrode arrays while a mug with 100 mL water was grasped and tilted towards various angles. The average impedance responses captured with each of the injecting electrode pairs is mapped to a pixelized heatmap.

pair recorded both the signal amplitude and phase shift. We conducted data collection while the sensorized gripper grasped an empty mug (representing the absence of liquid, i.e., air), as well as with 8 different liquids: water, electrolyte water, milk, energy drink, isopropanol (IPA), liquor, oil, and smoothie. In total, we collected 900 full swept-frequency data samples in 90 rounds over 3 days. We split the data in a conventional 80/20 manner for the training and validation of the liquids classifier.

With a frequency-specific impedance measuring setup, we collected impedance responses from all pairs of electrodes at 50 kHz. Using a 4 x 8 electrode matrix, we captured 256 readings in one full scan at the frame rate of 10 Hz. The measurements were taken layer by layer (4 layers in total). Each adjacent electrode pair within one layer was rotating as the AC signal injecting pair. The impedance responses were measured and recorded by all other adjacent pairs (8 injecting electrode pairs×8 measuring electrode pairs = 64 measurements per layer). Our data collection process involved the sensorized gripper securely holding a mug containing water. To introduce variations in the liquid's state, we systematically rotated the mug along different axes, covering a diverse set of angles. These rotations were carried out using a known rotation matrix, which was employed to generate the mathematical ground truth for the liquid state. In total, we collected 6600 data samples with 110 different rotation matrices (evenly distributed among 8-point compass roses) over 5 days. We randomly chose data from 88 rotations to train the liquid state estimator and used the remaining data from the unseen 22 rotations as validation and test sets.

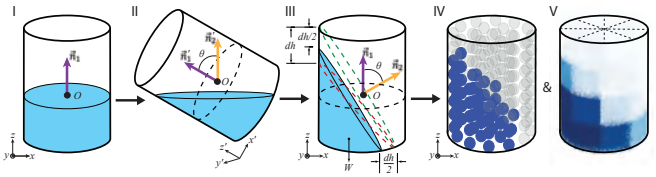

Fig. 6. **Ground truth generation.** The liquid states at the initial position (I) and tilted angles (II) are shown in sky blue. The liquid state is projected to the initial frame (III), where the ground truth was sampled and generated (IV & V). Normal vectors and calculated parameters are indicated.

D. Ground Truth Generation

Ground truth generation for liquid state estimation is calculated mathematically based on the known rotation of the robotic arm, the geometry of the container, and the volume of the introduced liquid. The robotic arm's interface gives the axis-angle representation of the pose, which can be converted into the rotation matrix R between the initial position and the rotated position of the container. The normal vector of the liquid surface at the initial position is defined as $\vec{n}_1 = (0, 0, 1)$ in the xyz coordinates such that the liquid surface is parallel to the world xy-plane and the height of the liquid along the z axis (Fig. 6.I). The center of the liquid surface is denoted as O. When the robotic gripper grasps the liquid container and rotates (Fig. 6 II), the liquid state changes while the liquid surface still remains parallel to the world xy-plane to form a cylindrical segment. The normal vector of the liquid surface at the rotated position can be defined as $\vec{n}_2' = (0, 0, 1)$ in the xyz coordinates. We project the rotated liquid to the xyz coordinates by applying the inverse of the rotation matrix between the initial xyz coordinates and the rotated $x'y'z'$ coordinates. Then, the normal vector of the rotated liquid surface can be calculated as $\vec{n}_2 = R^T \vec{n}_2'$ (Fig. 6.III). With $\vec{n}_1$ and $\vec{n}_2$, the angle of a rotation can be calculated as:

$$\theta = \arccos\left(\frac{\vec{n}_1 \cdot \vec{n}_2}{|\vec{n}_1||\vec{n}_2|}\right) \tag{1}$$

The liquid surface can be defined as the plane $Z_{water}(x, y)$ with respect to the normal vector of the rotated liquid surface $\vec{n}_2$, and the center of the liquid surface at the initial position (O), using the scalar equation of the plane [35].

This model overestimates both the total liquid volume and the heights of the liquid surfaces when the rotation angles surpass a certain threshold when the liquid does not entirely fill the base of the container and form a cylindrical wedge W (shown as a dashed green circle in Figure 6 III). To compensate for this overestimation and refine the heights of the liquid surfaces, the derived equation of the plane of the liquid surface should be shifted. The z-intercept is first adjusted by decreasing dh such that the volume of (W) is the same as the volume of the introduced liquid (i.e., 100 mL) while keeping the base-intercept unchanged (shown as a dashed red circle). dh can be derived from the equation on the volume of the cylindrical wedge [36].

Since dh is a relatively small value, we assume that θ remains constant after the adjustment. In other words, the shifts in the z- & base- intercept approximately contribute equally to the overall volume change. Therefore, the liquid surface plane $Z_{water}(x, y)$ is shifted by $\frac{dh}{2}$ along $-z$ axis. This adjustment reduces the root-mean-squared error (RMSE) of volume estimation from 2.860 to 0.265 mL in a 100 mL liquid volume case, yielding a better liquid state estimation.

Given the liquid surface plane $Z_{water}(x, y)$, ground truth are generated in both binary and continuous forms. We first generate sample points (S_b) in the volume, for example, 152 points evenly along 8 height layers with 19 evenly distributed points within each height layer. We then assign binary values representing the existence of water (0 as "no-water-present" and 1 as "water-present") by comparing the Cartesian coordinates (x_b, y_b, z_b) of each sampled point with the height of the liquid surface $Z_{water}(x_b, y_b)$.

We also generate continuous ground truth data representing the water composition within various regions of the volume, by slicing the volume of the container into 4×8 wedges (corresponds to the 4×8 electrode array) and sample 1000 uniformly distributed random points (S_p^i, where i corresponds to the count of sliced wedges) within each wedge. The Cartesian coordinate (x_p^i, y_p^i, z_p^i) of each sampled points is compared to the liquid surface plane $Z_{water}(x_p^i, y_p^i)$. We then allocate the points percentage located beneath the liquid surface to each wedge with continuous values (from 0 to 1), representing the amount of liquid present within each wedge.

E. Model Architecture

Our liquid state estimation model takes in a scan of impedance reading across all electrode pairs (256 measurements, more details in Section III.C) and predicts the probability of the presence of water at the sampled location. The input of the model is a three-dimensional vector with the size of [8, 8, 4], which represents 8 impedance measurements from each of the 8 different injecting electrode pairs, along 4 individual electrode layers. The output of the model is a 1D vector with a size of sampled ground truth. Our model has two 2D convolutional layers, followed by a fully connected layer after flattening. The entire model has 196,214 parameters, a suitable size for on-device inference. Each of the convolutional layers uses 8 and 16 3×3 kernels and zero padding to keep the dimension the same, with ReLU as the activation function. The model was trained by minimizing the mean-squared error (MSE) via Adam optimizer [37] with a learning rate of 0.001 and a batch size of 128.

Similarly, our liquid classifier takes in a frequency-swept impedance sensing sequence and outputs the probabilities of each liquid class. The input of this model is a two-dimensional vector with the size of [100, 2], which corresponds to amplitude and phase shift readings in 100 steps of frequency sweep impedance measurements (between 5 kHz and 500 kHz). The liquids classifier consists of two fully-connected layers, with 32 and 9 neurons each. The first layer uses ReLU as the activation function, and the second layer uses soft-max for generating the classification results. Both layers use L1 regularization with a 0.01 regularization factor. The model was trained by minimizing categorical cross-entropy loss using Adam optimizer with a learning rate of 0.001. Both models were implemented in TensorFlow [38].

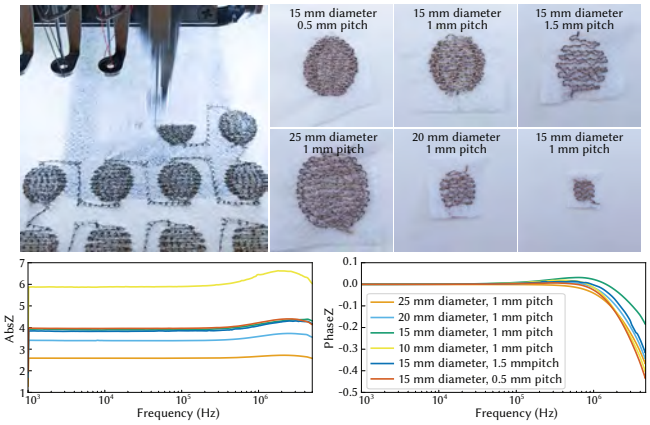

Fig. 7. **Embroidered electrode designs and characterization.** Impedance measurements were conducted across various frequencies using embroidered electrodes featuring distinct sizes and stitch spacing.

IV. RESULTS

In this section, we present results on embroidered electrode characterization, the model performances on liquids classification and state estimation, and results on a series of ablation studies to evaluate our framework effectiveness.

A. Embroidered electrode characterization

We characterized the embroidered electrode using an impedance analyzer (Zurich Instruments MFIA) with a frequency sweep between 1 kHz and 5 MHz (500 steps). As demonstrated in Fig. 7, the impedance across frequencies decreases as the electrode sizes increase. However, the impedance remains stable despite an increase in embroidery pitches, which indicates that the density of conductive traces has minimal effect on the signal transmission. We employed the embroidered electrode with 1 mm pitch and 10 mm diameter in our final design for the gripper, featuring a 4×4 sensing electrode matrix. The 10 mm diameter was chosen due to the constraints in the gripper geometry and the conservative wire spacing of 3 mm with our fabrication resolution. The 1 mm pitch was chosen to expedite the fabrication process while maintaining stable electrical performance.

B. Liquid Classification

Our liquid classification model identifies 9 liquid classes, including air, water, electrolyte water, milk, energy drink, IPA, liquor, oil, and smoothie in a grasped container with an accuracy of 93.33%. Based on the confusion matrix (Fig. 8), the most confusing cases occur between air (i.e., empty mug) and water. This is likely because we used deionized water with little to no free electrons in it, which is verified by the resistance measurement in Megaohms ranges via a DC multimeter. During impedance sensing, water behaves akin to air over its real component, like an insulator. Consequently, distinctions between the two primarily manifest in the imaginary component, in contrast to other liquid types that exhibit disparities in both real and imaginary readings.

C. Liquid State Estimation

In general, we performed liquid state estimation with both a classification setup and a regression setup. In the

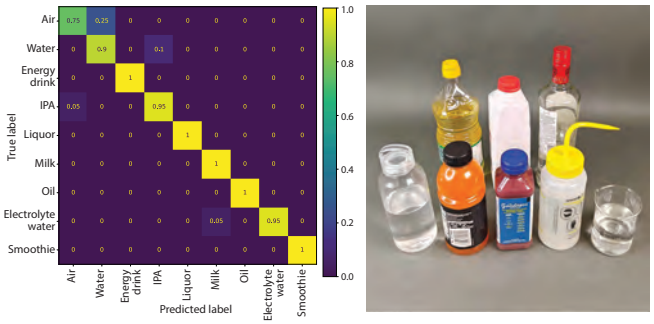

Fig. 8. **Confusion matrix on liquids classification.**

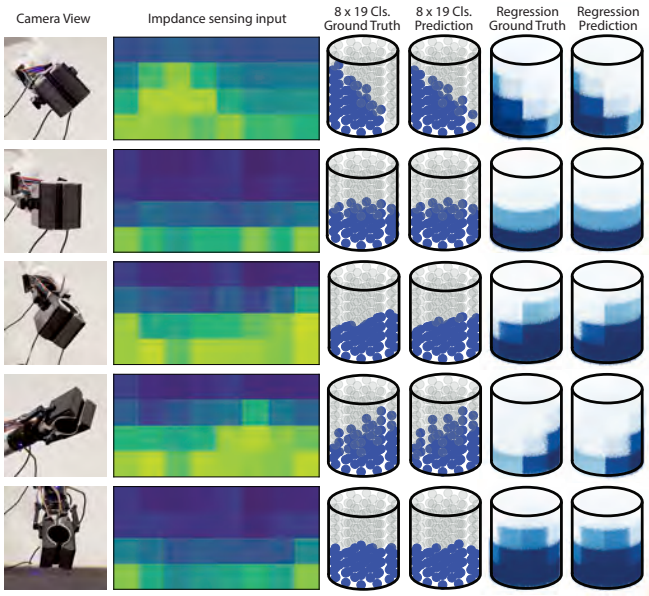

Fig. 9. **Results on liquid state estimation.** From left to right columns: camera view of gripper and liquid container tilting degrees, EIT sensing raw signal, 8×19 binary classification ground truth and prediction results, 32-wedge (4×8) regression ground truth and prediction results.

classification setup, the model was supervised by ground-truth labels in the form of an 8×19 binary array. The model was expected to categorize each of the 8×19 data points into one of two categories: either "water-present" or "no-water-present." In this configuration, our model achieved a classification accuracy of 97.65%. On the other hand, in the regression setup, the model was supervised by 32 continuous numerical values, representing the percentage of water presence in each of the 4×8 wedges. Our model obtained a mean-squared error (MSE) of 7.46e-5. The corresponding camera views, impedance sensing inputs, and ground-truth values are generated from mathematical analysis (Figure. 8).

We investigated the effectiveness of our impedance sensors and modeling pipeline with respect to the sampled resolution along the circular, height, and inner/outer directions. More specifically, we supervised the model with ground truth that was sampled with various resolutions along the circular direction and the height direction (Fig. 10 left). We trained models using ground truth data sampled at various height layers, ranging from 4 (i.e., a number of layers in our sensor electrode matrix) to 16. A consistent configuration with 19 evenly distributed points within the circular plane at each height layer were maintained. The model demonstrates robust

performance with data sampled up to 8 sampled height layers but experiences a significant accuracy drop when moving to 16 layers. Likewise, we trained models with ground truth sampled with 10, 19, and 38 evenly distributed points within the circular plane at 8 individual height layers. No discernible performance difference was observed between models trained with 10 and 19 points along the circular direction, which indicates the capability of our sensors and models. A significant drop in accuracy appeared with further resolution increases along a circular direction to 38 points.

It is noteworthy that models trained with ground truth data sampled using varying radii (8×19 V), where points were uniformly distributed across each layer plane with most points not in direct contact with the sensing patch, and models trained with a single fixed radius (8×19 S), where all points were distributed along the circumference and in direct contact with the sensing patch, yield remarkably similar accuracy results (less than 0.4%). This similarity suggests that despite our impedance sensing electrodes being affixed only to the exterior of the mug, they are capable of effectively extracting data points located within inner circular regions, all without requiring direct contact or connecting traces to the electrodes. Also, we achieved an accurate state estimation with a resolution up to 8×19, effectively doubling the resolution of our impedance sensing matrix (4×8) in both circular and height directions. This increase in resolution can be attributed to the continuous flow of the liquid, enabling the model to effectively interpolate between neighboring sampled points. Additionally, it underscores the inherent capability of impedance sensing to comprehensively capture information across entire planar surfaces.

D. Ablation Study

We performed an ablation study on the sensing resolution of the impedance sensing array. More specifically, to ablate the impedance sensing resolution, we reassign values in every two or four cells with the average of their values. We reduced the effective sensing resolution from 4×8×8 to 4×8×4 and 4×8×2 along the circular direction, as well as from 4×8×8 to 2×8×8 and 1×8×8 along the vertical height direction. We then applied the same training pipeline to derive the predictions, as shown in Fig. 10 right. Overall, our sensing resolution is more robust along the circular direction, as indicated by the 81.81% accuracy with only 2 effective sensor readings per height layer, and can be more delicate along the vertical height resolution for liquid state estimation.

V. DISCUSSION

Currently, our data collection primarily focuses on scenarios involving static liquid conditions. Specifically, we programmed the robotic arm to rotate and pause at a series of pre-defined angles. Although we tried to cover as many different degrees as possible along the 8-point compass roses based on the rotation resolution of the robotic arm, we did not include scenarios involving vigorous liquid movements. Such movements would introduce intricate liquid dynamics and sloshing, which were not part of our data collection

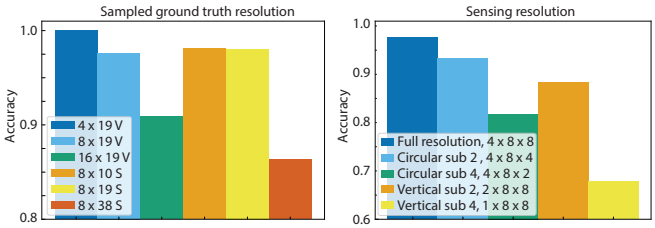

Fig. 10. **Model evaluation and ablation study.** Left, model effectiveness regards to prediction resolution along circular and height directions. Right, Ablation study on effective impedance sensing resolution along circular and height directions. V represents points sampled along various radii and S represents points sampled along a single radius.

approach. We focused on static scenarios at the current stage because our generative models encompass various liquid types, and incorporating liquid sloshing would introduce numerous additional parameters related to fluid properties, arm movement dynamics, and container geometries. Also, in order to capture the impedance reading of all electrode pairs for liquid sloshing states at a reasonable temporal resolution for model training, we estimated the impedance sensing data acquisition frame rate should be around 100Hz based on previous works [39], while we can only achieve a maximum frame rate of 15.62 Hz with the current setup.

For future work, we are planning to extend our approach to containers with more diverse geometries via our customizable and adaptive sensor designs. We plan to improve the impedance sensing frame rate to capture inter-degree liquid behavior, which will enable the capturing of fine-grained liquid movement and dynamics. Moreover, we plan to integrate our pipeline with physics-based liquid simulations, such as voxel method and fluid simulation, which will offer quick and rich data collection featuring fine details, including liquid sloshing and splashing. This will help with the development of a more delicate liquid state estimation model. We will also expand our liquid classification techniques to analyze the liquid properties such as viscosity and temperature. We are aiming to combine our liquid classification and state estimation pipeline with closed-loop control algorithms to provide real-time sensing feedback and liquid state estimation to facilitate real-world robotics manipulation tasks.

VI. CONCLUSION

In this study, we introduce a novel approach for liquid type identification and state estimation using impedance sensing. We devised scalable, customizable embroidered electrode arrays, seamlessly integrated with a portable impedance sensing board compatible with various robot grippers. Our dataset comprises over 900 swept-frequency liquid type measurements and 110 degrees of liquid state data. We developed machine learning models for liquid identification (93.33%) & state estimation (97.65%). Additionally, we evaluated sensor effectiveness, sensing array resolution, conducted an ablation study, and discussed system limitations and future prospects.

ACKNOWLEDGMENT

We acknowledge support from MIT-GIST Joint Program, Toyota Research Institute, and Wistron.

REFERENCES

[1] J. Cui and J. Trinkle, "Toward next-generation learned robot manipulation," *Science robotics*, vol. 6, no. 54, p. eabd9461, 2021.

[2] Y. Luo, Y. Li, P. Sharma, W. Shou, K. Wu, M. Foshey, B. Li, T. Palacios, A. Torralba, and W. Matusik, "Learning human–environment interactions using conformal tactile textiles," *Nature Electronics*, vol. 4, no. 3, pp. 193–201, 2021.

[3] A. Zeng, S. Song, K.-T. Yu, E. Donlon, F. R. Hogan, M. Bauza, D. Ma, O. Taylor, M. Liu, E. Romo, *et al.*, "Robotic pick-and-place of novel objects in clutter with multi-affordance grasping and cross-domain image matching," *The International Journal of Robotics Research*, vol. 41, no. 7, pp. 690–705, 2022.

[4] A. Zeng, S. Song, S. Welker, J. Lee, A. Rodriguez, and T. Funkhouser, "Learning synergies between pushing and grasping with self-supervised deep reinforcement learning," in *2018 IEEE/RSJ International Conference on Intelligent Robots and Systems (IROS)*. IEEE, 2018, pp. 4238–4245.

[5] Z. Xian, B. Zhu, Z. Xu, H.-Y. Tung, A. Torralba, K. Fragkiadaki, and C. Gan, "Fluidlab: A differentiable environment for benchmarking complex fluid manipulation," *arXiv preprint arXiv:2303.02346*, 2023.

[6] R. Sanchez-Matilla, K. Chatzilygeroudis, A. Modas, N. F. Duarte, A. Xompero, P. Frossard, A. Billard, and A. Cavallaro, "Benchmark for human-to-robot handovers of unseen containers with unknown filling," *IEEE Robotics and Automation Letters*, vol. 5, no. 2, pp. 1642–1649, 2020.

[7] C. Matl, R. Matthew, and R. Bajcsy, "Haptic perception of liquids enclosed in containers," in *2019 IEEE/RSJ International Conference on Intelligent Robots and Systems (IROS)*. IEEE, 2019, pp. 7142–7149.

[8] S. Chitta, J. Sturm, M. Piccoli, and W. Burgard, "Tactile sensing for mobile manipulation," *IEEE Transactions on Robotics*, vol. 27, no. 3, pp. 558–568, 2011.

[9] N. Hanson, W. Lewis, K. Puthuveetil, D. Furline, A. Padmanabha, T. Padir, and Z. Erickson, "Slurp! spectroscopy of liquids using robot pre-touch sensing," in *2023 IEEE International Conference on Robotics and Automation (ICRA)*. IEEE, 2023, pp. 3786–3792.

[10] H.-J. Huang, X. Guo, and W. Yuan, "Understanding dynamic tactile sensing for liquid property estimation," *arXiv preprint arXiv:2205.08771*, 2022.

[11] F. Zhu, R. Jia, L. Yang, Y. Yan, Z. Wang, J. Pan, and W. Wang, "Visual-tactile sensing for real-time liquid volume estimation in grasping," in *2022 IEEE/RSJ International Conference on Intelligent Robots and Systems (IROS)*. IEEE, 2022, pp. 12 542–12 549.

[12] K. Yano, T. Toda, and K. Terashima, "Sloshing suppression control of automatic pouring robot by hybrid shape approach," in *Proceedings of the 40th IEEE Conference on Decision and Control (Cat. No.01CH37228)*, vol. 2, Dec 2001, pp. 1328–1333 vol.2.

[13] M. Tamosiunaite, B. Nemec, A. Ude, and F. Wörgötter, "Learning to pour with a robot arm combining goal and shape learning for dynamic movement primitives," *Robotics and Autonomous Systems*, vol. 59, no. 11, pp. 910–922, 2011. [Online]. Available: https://www.sciencedirect.com/science/article/pii/S0921889011001254

[14] L. Rozo, P. Jiménez, and C. Torras, "Force-based robot learning of pouring skills using parametric hidden markov models," in *9th International Workshop on Robot Motion and Control*, July 2013, pp. 227–232.

[15] A. Yamaguchi and C. G. Atkeson, "Stereo vision of liquid and particle flow for robot pouring," in *2016 IEEE-RAS 16th International Conference on Humanoid Robots (Humanoids)*, Nov 2016, pp. 1173–1180.

[16] C. Schenck and D. Fox, "Visual closed-loop control for pouring liquids," in *2017 IEEE International Conference on Robotics and Automation (ICRA)*, May 2017, pp. 2629–2636.

[17] R. Mottaghi, C. Schenck, D. Fox, and A. Farhadi, "See the glass half full: Reasoning about liquid containers, their volume and content," in *2017 IEEE International Conference on Computer Vision (ICCV)*, Oct 2017, pp. 1889–1898.

[18] L. Zlokapa, Y. Luo, J. Xu, M. Foshey, K. Wu, P. Agrawal, and W. Matusik, "An integrated design pipeline for tactile sensing robotic manipulators," in *2022 International Conference on Robotics and Automation (ICRA)*. IEEE, 2022, pp. 3136–3142.

[19] K. Liu, Y. Wu, S. Wang, H. Wang, H. Chen, B. Chen, and J. Yao, "Artificial sensitive skin for robotics based on electrical impedance tomography," *Advanced Intelligent Systems*, vol. 2, no. 4, p. 1900161, 2020.

[20] R. Harikumar, R. Prabu, and S. Raghavan, "Electrical impedance tomography (eit) and its medical applications: A review," 2013.

[21] J. Zhu, J. C. Snowden, J. Verdejo, E. Chen, P. Zhang, H. Ghaednia, J. H. Schwab, and S. Mueller, "Eit-kit: An electrical impedance tomography toolkit for health and motion sensing," in *The 34th Annual ACM Symposium on User Interface Software and Technology*, 2021, pp. 400–413.

[22] J. Zhu, Y. Lei, A. Shah, G. Schein, H. Ghaednia, J. Schwab, C. Harteveld, and S. Mueller, "Musclerehab: Improving unsupervised physical rehabilitation by monitoring and visualizing muscle engagement," in *Proceedings of the 35th Annual ACM Symposium on User Interface Software and Technology*, 2022, pp. 1–14.

[23] X. Liu, J. Liu, Z. Du, Q. Zhao, J. Zhao, and Y. Huang, "The research on non-destructive testing method of sheet resistance in micro area of silicon wafer based on eit technology," 09 2008, pp. 1494 – 1497.

[24] D. Silvera-Tawil, D. Rye, M. Soleimani, and M. Velonaki, "Electrical impedance tomography for artificial sensitive robotic skin: A review," *IEEE Sensors Journal*, vol. 15, no. 4, pp. 2001–2016, 2015.

[25] T. Mukai, S. Hirano, H. Nakashima, Y. Kato, Y. Sakaida, S. Guo, and S. Hosoe, "Development of a nursing-care assistant robot riba that can lift a human in its arms," in *2010 IEEE/RSJ International Conference on Intelligent Robots and Systems*. IEEE, 2010, pp. 5996–6001.

[26] D. S. Tawil, D. Rye, and M. Velonaki, "Touch modality interpretation for an eit-based sensitive skin," in *2011 IEEE International Conference on Robotics and Automation*. IEEE, 2011, pp. 3770–3776.

[27] G. H. Büscher, R. Kõiva, C. Schürmann, R. Haschke, and H. J. Ritter, "Flexible and stretchable fabric-based tactile sensor," *Robotics and Autonomous Systems*, vol. 63, pp. 244–252, 2015.

[28] Y. Wu, D. Jiang, X. Liu, R. Bayford, and A. Demosthenous, "A human–machine interface using electrical impedance tomography for hand prosthesis control," *IEEE Transactions on Biomedical Circuits and Systems*, vol. 12, no. 6, pp. 1322–1333, 2018.

[29] O. Kanoun, A. Y. Kallel, H. Nouri, B. B. Atitallah, D. Haddad, Z. Hu, M. Talbi, A. Al-Hamry, R. Munja, F. Wendler, R. Barioul, T. Keutel, and A. Mangler, "Impedance spectroscopy: Applications, advances and future trends," *IEEE Instrumentation & Measurement Magazine*, vol. 25, no. 3, pp. 11–21, 2022.

[30] M. Koseoglou, E. Tsioumas, D. Papagiannis, N. Jabbour, and C. Mademlis, "A novel on-board electrochemical impedance spectroscopy system for real-time battery impedance estimation," *IEEE Transactions on Power Electronics*, vol. 36, no. 9, pp. 10 776–10 787, 2021.

[31] Y. Ding, H. Kisner, T. Kong, and U. Thomas, "Using machine learning for material detection with capacitive proximity sensors," in *2020 IEEE/RSJ International Conference on Intelligent Robots and Systems (IROS)*, 2020, pp. 10 424–10 429.

[32] Y. Ding, H. Zhang, and U. Thomas, "Capacitive proximity sensor skin for contactless material detection," in *2018 IEEE/RSJ International Conference on Intelligent Robots and Systems (IROS)*, 2018, pp. 7179–7184.

[33] M. Sato, I. Poupyrev, and C. Harrison, "Touché: Enhancing touch interaction on humans, screens, liquids, and everyday objects," in *Proceedings of the SIGCHI Conference on Human Factors in Computing Systems*, ser. CHI '12. New York, NY, USA: Association for Computing Machinery, 2012, p. 483–492. [Online]. Available: https://doi.org/10.1145/2207676.2207743

[34] Y. Luo, K. Wu, A. Spielberg, M. Foshey, D. Rus, T. Palacios, and W. Matusik, "Digital fabrication of pneumatic actuators with integrated sensing by machine knitting," in *Proceedings of the 2022 CHI Conference on Human Factors in Computing Systems*, 2022, pp. 1–13.

[35] "Equation of a Plane - Wolfram Demonstrations Project — demonstrations.wolfram.com," https://demonstrations.wolfram.com/EquationOfAPlane/, [Accessed 15-09-2023].

[36] J. W. Harris, *"Obliquely Cut Circular Cylinder" and "Segment of a Cylinder."*. Springer-Verlag, 1998, p. 103–104.

[37] D. P. Kingma and J. Ba, "Adam: A method for stochastic optimization," *arXiv preprint arXiv:1412.6980*, 2014.

[38] M. Abadi, A. Agarwal, P. Barham, E. Brevdo, Z. Chen, C. Citro, G. S. Corrado, A. Davis, J. Dean, M. Devin, S. Ghemawat, I. Goodfellow, A. Harp, G. Irving, M. Isard, Y. Jia, R. Jozefowicz, L. Kaiser, M. Kudlur, J. Levenberg, D. Mané, R. Monga, S. Moore, D. Murray, C. Olah, M. Schuster, J. Shlens, B. Steiner, I. Sutskever, K. Talwar, P. Tucker, V. Vanhoucke, V. Vasudevan,

F. Viégas, O. Vinyals, P. Warden, M. Wattenberg, M. Wicke, Y. Yu, and X. Zheng, "TensorFlow: Large-scale machine learning on heterogeneous systems," 2015, software available from tensorflow.org. [Online]. Available: https://www.tensorflow.org/

[39] X. Luo, A. Kareem, L. Yu, and S. Yoo, "A machine learning-based characterization framework for parametric representation of liquid sloshing," *Results in Engineering*, vol. 18, p. 101148, 2023. [Online]. Available: https://www.sciencedirect.com/science/article/pii/S259012302300275X